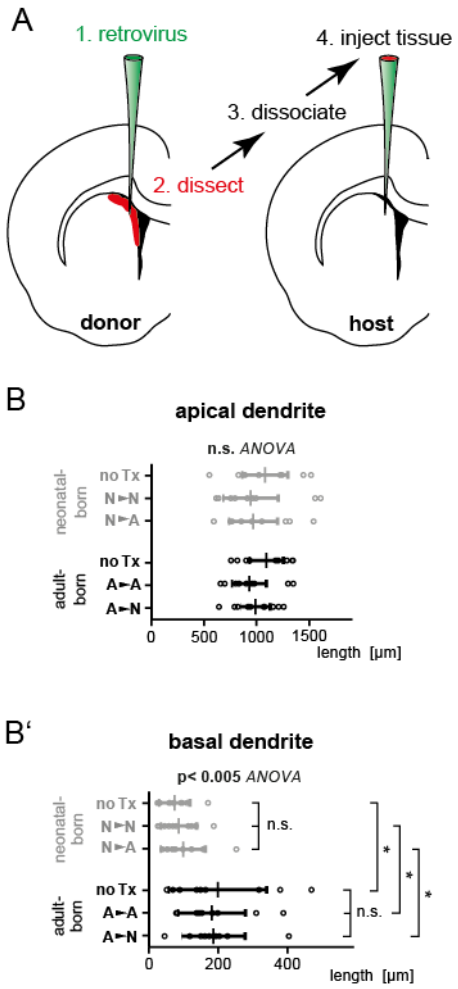

Fig. S1. Transplantation and dendritic length of grafted GCs. (A) Scheme of the transplantation procedure showing the viral injection, dissociation, and transplantation site, respectively. (B-B') Length (mean and 95% confidence interval) of the total apical (B) and basal dendrite (B') of non-transplanted (no Tx) GCs and transplanted GCs at 28 dpi (n=10 GCs per condition, ANOVA followed by posttest (* P<0.05)).

Note: The longer basal dendrites in GCs generated from the adult are explained by the observations that GCs with somata located deeper in the GC layer have longer basal dendrites (e.g. Kelsch et al. (2012) J. Comp. Neurol. 520:1327-38). Importantly, more deep GCs are generated in the adult SVZ. To confirm this observation for transplanted GCs, all neurons in (B') were split into GCs with cell bodies in the lower half of the GC layer (deep GCs) and superficial GCs with somata in the upper half of the GC layer closer to the mitral cell layer. Pooled superficial GCs had similar basal dendrite length independent of whether they were generated from neonatal or adult precursors (65±6 vs. 71±7 µm, n=22 and 6 GCs; n.s., t-test). Similarly, GCs with deep somata generated from neonatal or adult precursors had a similar basal dendrite length (156±18 vs. 221±20 µm, n=8 and 24 GCs; n.s., t-test).

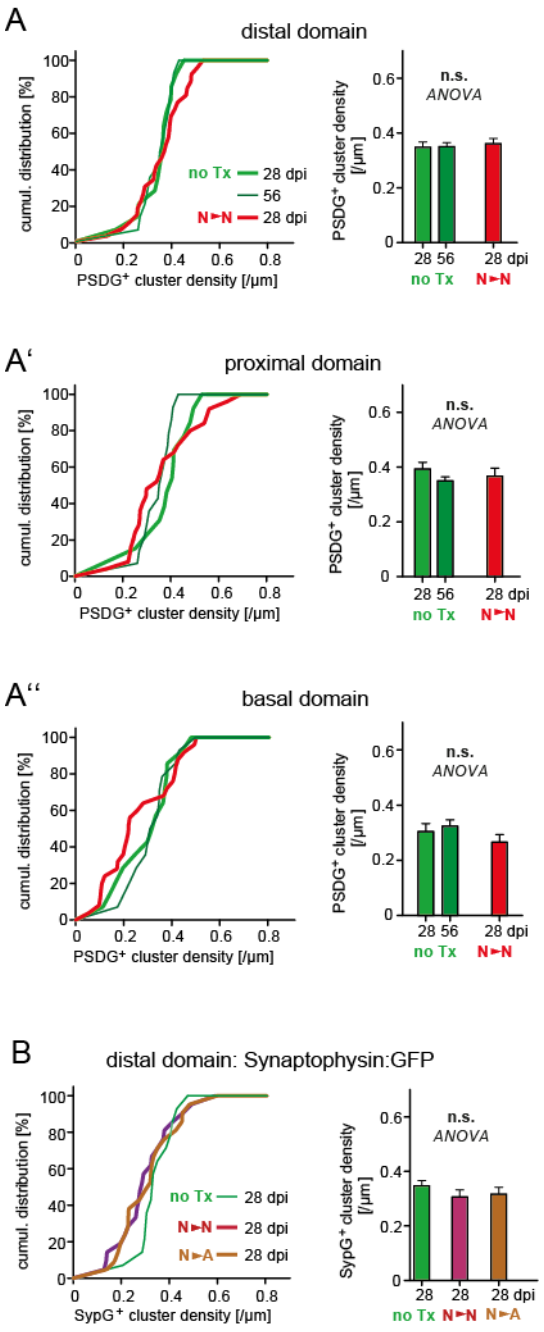

Fig. S2. Organization of glutamatergic input synapses of GCs derived from neonatal precursors. (A-A'') Cumulative plots of PSDG$^+$ cluster densities in the distal (A), proximal (A'), and basal domain (A'') for non-transplanted (no Tx) neonatal-born GCs at 28 and 56 dpi (n=14 GCs for each plotted time point) and the N→N condition at 28 dpi shown in Fig. 4C. Right: Statistical comparison (mean±s.e.m.) of the data shown on the left (ANOVA). (B) Cumulative plots of SypG$^+$ clusters that label presynaptic output synapses in the distal domain of for no Tx neonatal-born, N→N and N→A GCs at 28 dpi (n=14, 25, 25 GCs, respectively). Right: Statistical comparison (mean± s.e.m.) of the data shown on the left (ANOVA).

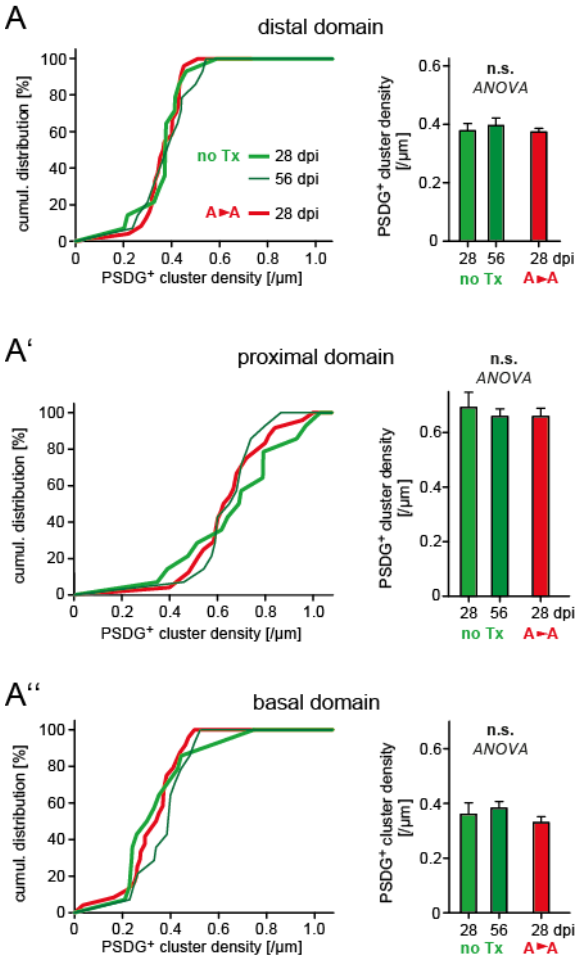

Fig. S3. Synaptic organization of GCs derived from adult precursors. (A-A'') Cumulative plots of PSDG$^+$ cluster densities in the distal (A), proximal (A'), and basal domain (A'') for non-transplanted (noTx) adult-born GCs at 28 and 56 dpi (n=14 GCs, respectively) and the A→A condition at 28 dpi shown in Fig. 5C. Right: Statistical comparison (mean± s.e.m.) of the data shown on the left (ANOVA).

Note: For the data shown in (A), we performed additional analysis for non-transplanted adult-born GCs. In the distal domain, PSDG$^+$ cluster densities tended to increase between 28 and 56 dpi (n.s., t-test), while in the same dendritic segments the density of protrusions tended to decrease (28 dpi: 0.361±0.025/µm and 56 dpi: 0.335±0.023/µm; n=14 GCs, n.s., t-test). However, the difference between the PSDG$^+$ cluster density and the spine density in the same neurons increased significantly from 28 to 56 dpi (28 dpi: 0.016±0.002/µm and 56 dpi: 0.061±0.010/µm; n=14 GCs, p=0.0002, t-test).

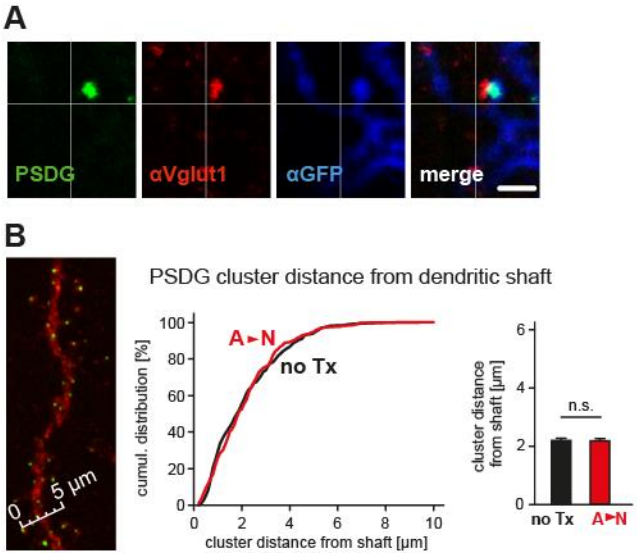

Fig. S4. PSD-95:GFP distribution along distal dendrites of A→N GCs and its presynaptic contact. (A) In the distal domain of A→N GCs at 28 dpi, PSDG$^+$ clusters were contacted by a presynaptic marker, Vglut1 (scale bar 3 µm). (B) Left: Measurement of the distance of PSDG$^+$ clusters from the dendritic shaft in the distal domain in maximum density projection (scale bar 5 µm). Middle: Cumulative plots of the distance of PSDG$^+$ clusters from the dendritic shaft in the distal domain of non-transplanted (no TX) adult-born GCs and A→N GCs at 28 dpi (total number of clusters analyzed: 436 and 315 in 10 GCs, respect.). Right: Statistical comparison (mean± s.e.m.) of the data shown to the left (t-test).